

Room-temperature ferromagnetism in Cu-implanted 6H-SiC single crystal

H. W. Zheng, Y. L. Yan, Z. C. Lv, S. W. Yang, X. G. Li, J. D. Liu, B. J. Ye, C. X. Peng, C. L. Diao, and W. F. Zhang

Citation: [Applied Physics Letters](#) **102**, 142409 (2013); doi: 10.1063/1.4800562

View online: <http://dx.doi.org/10.1063/1.4800562>

View Table of Contents: <http://scitation.aip.org/content/aip/journal/apl/102/14?ver=pdfcov>

Published by the [AIP Publishing](#)

Articles you may be interested in

[Room-temperature ferromagnetism in hydrogenated ZnO nanoparticles](#)

J. Appl. Phys. **115**, 033902 (2014); 10.1063/1.4862306

[Magnetic properties of Mn-implanted 6H-SiC single crystal](#)

J. Appl. Phys. **111**, 07C315 (2012); 10.1063/1.3677870

[Strong room-temperature ferromagnetism in Cu-implanted nonpolar GaN films](#)

J. Appl. Phys. **106**, 113921 (2009); 10.1063/1.3266013

[Room-temperature ferromagnetism of Cu-implanted GaN](#)

Appl. Phys. Lett. **90**, 032504 (2007); 10.1063/1.2431765

[Fluence, flux, and implantation temperature dependence of ion-implantation-induced defect production in 4H-SiC](#)

J. Appl. Phys. **97**, 033513 (2005); 10.1063/1.1844618



Room-temperature ferromagnetism in Cu-implanted 6H-SiC single crystal

H. W. Zheng,¹ Y. L. Yan,¹ Z. C. Lv,¹ S. W. Yang,² X. G. Li,² J. D. Liu,³ B. J. Ye,³ C. X. Peng,¹ C. L. Diao,¹ and W. F. Zhang^{1,a)}

¹Department of Physics, Institute of Microsystem, Key Lab for Photovoltaic Materials of Henan Province, Henan University, Kaifeng 475004, China

²Department of Physics, Hefei National Laboratory for Physics Sciences at the Microscale, University of Science and Technology of China, Hefei 230026, China

³Department of Modern Physics, University of Science and Technology of China, Hefei 230026, China

(Received 18 February 2013; accepted 25 March 2013; published online 12 April 2013)

200 keV Cu⁺ ions were implanted into 6H-SiC single crystal at room temperature with fluence of $8 \times 10^{15} \text{ cm}^{-2}$. No ferromagnetism (FM)-related secondary phase was found by the results of high-resolution x-ray diffraction and x-ray photoelectron spectroscopy. Positron annihilation lifetime spectroscopy results indicated that the main defect type was silicon vacancy and the concentration of it increased after Cu implantation. The room-temperature ferromagnetism was detected by superconducting quantum interference device. First-principles calculations revealed that the magnetic moments mainly come from the 2p orbitals of C atoms and 3d orbitals of Cu dopant. The origin of the FM has been discussed in detail. © 2013 American Institute of Physics. [<http://dx.doi.org/10.1063/1.4800562>]

Diluted magnetic semiconductors (DMSs) have attracted lots of attention due to their applications in spintronic devices.^{1,2} SiC-based DMSs are highly desired in the application of high-power devices due to high electric breakdown field of SiC.³⁻⁵ Among various methods for fabricating SiC-based DMSs, ion implantation, a convenient method in incorporating impurities into semiconductors at non-equilibrium conditions, is being practiced for a long time. Magnetic properties of Fe, Ni, and Mn implanted SiC have been reported.⁶ However, it is still indistinct whether the observed ferromagnetism (FM) in DMSs is an inherent property or from secondary precipitates. Cu stands out as a prominent transition metal because metallic copper and all possible Cu-based second phases are nonmagnetic, thus clustering does not lead to parasitic magnetic signals.⁷ Although magnetic properties of Cu-doped SiC have been predicted theoretically,^{8,9} experimental observation of FM in Cu-doped 3C-SiC films has been little addressed.⁹ In this letter, Cu-doped 6H-SiC with room-temperature FM has been fabricated using ion implantation. Moreover, FM origin has also been fully discussed.

One-side polished 6H-SiC (0001) single crystals from the KMT Corporation (Hefei, China) have been implanted with Cu⁺ ions with an energy of 200 keV and a dose of $8 \times 10^{15} \text{ cm}^{-2}$ at room temperature. The direction of the incident ion beam was tilted by 7° to surface normal to reduce possible channeling effect. During the implantation, the beam current density was kept at $1 \mu\text{A cm}^{-2}$ and the estimated temperature rise of the wafers was about 30 °C. The samples were subsequently subjected to a rapid thermal annealing (RTA) at 850 °C for 15 min under flowing N₂ protection. By using the stopping and range of ions in matter (SRIM) calculation, the created damage profile is about 200 nm and the Cu peak concentrations are about 1.85 at. %. The structure and the defects were investigated by high

resolution x-ray diffractometry (HRXRD, D8 Discover, Bruker), x-ray photoelectron spectroscopy (XPS, ESCALAB 250, Thermo-VG Scientific), and positron annihilation lifetime spectroscopy (PALS), respectively. Magnetic properties were measured by superconducting quantum interface device (SQUID, MPMS XL-7). During magnetic measurements, magnetic field was parallel to the samples' plane.

Fig. 1(a) shows the HRXRD patterns for Cu-implanted 6H-SiC. As a reference, XRD pattern of unimplanted SiC was also given. For unimplanted SiC, the peak at $2\theta = 35.58^\circ$ can be easily indexed as (0006) plane of hexagonal SiC. Compared with unimplanted SiC, the position of (0006) peak for the Cu-implantation SiC shifts to smaller angle, which may be an indication of the incorporation of a partial amount of implanted Cu in the SiC lattice due to larger Cu covalent radius. Implantation-induced vacancies may be another origin of the observed shift.⁴ For the Cu-implanted 6H-SiC, no other significant features are observed except for the SiC peak, meaning no secondary phases can be detected with the limitation of the diffractometer.

To investigate the valence state of copper, XPS was taken for Cu 2p_{3/2} binding energy range for the Cu-implanted SiC samples, as shown in Fig. 1(b). The deconvolution of the core level was applied using Lorentzian fitting to determine various bonding compositions. The peak at 932.7 eV agrees well with Cu 2p_{3/2} for metallic Cu (Cu⁰), while the peak at 933.6 eV can be attributed to Cu-C bond.^{10,11} Therefore, it is deduced that partially implanted Cu ions are present in the form of Cu⁰ in the samples, and some Cu ions locate at substitutional Si sites in the 6H-SiC lattice. The process of the implantation and subsequent RTA were carried out at high vacuum or N₂ protection. Moreover, high-resolution XPS spectrum of O in the Cu⁺ implanted sample further eliminates the existence of copper oxide.

For investigating the defect types produced by ion-implantation, PALS measurements have been performed. The PALS were measured using a fast-fast coincidence

^{a)}Author to whom correspondence should be addressed. Electronic mail: wfzhang@henu.edu.cn. Tel./Fax: +86-378-3881602.

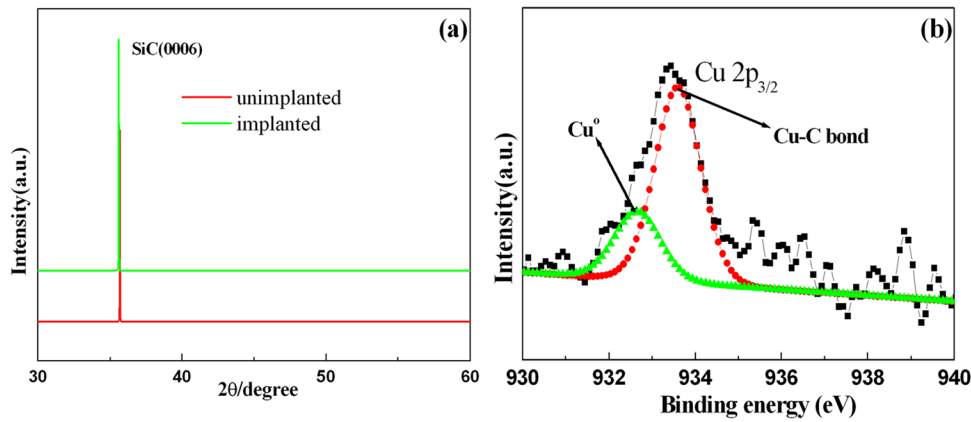


FIG. 1. (a) HRXRD patterns of unimplanted and Cu^+ -implanted 6H-SiC. (b) XPS image of $\text{Cu } 2p_{3/2}$ for Cu^+ -implanted 6H-SiC.

system, with a resolution of 230 ps. At least 10^6 events were collected in per spectrum. Each spectrum was fitted using the LIFETIME-9 package with the three-component fitting procedure.¹² The longest lifetime τ_3 and its intensity I_3 were over 1.7 ns and about 5%, respectively, without significant variation for the unimplanted and implanted samples. This component is attributed to the ortho-positronium (o-Ps) annihilation in the source and is ignored in our discussion. For the two samples, the lifetime τ_1 , τ_2 and its intensity are listed in Table I. It is observed that the lifetimes τ_1 and τ_2 are independent of implantation behavior within the allowed range, indicating that the nature of the vacancy defects has not changed with and without the implantation. The lifetime value of τ_1 is measured to show an almost constant value (≈ 170 ps), consistent with the positron lifetimes at silicon vacancy defect (V_{Si}) in 6H-SiC single crystal.¹³ Thus, lifetime τ_1 is assigned to positron trapping at V_{Si} . The lifetime value of τ_2 can conform to positron lifetime of vacancy clusters, similar to that of the prior theoretical calculation.¹⁴ I_1 value gets larger after the implantation, signifying the increasing concentration of V_{Si} . Similar phenomena about the increase of vacancy-type defects after implantation have also been reported.¹⁵ I_2 value decreases after implantation, indicating the collapse and shrinkage of the divacancies cluster and then the concentration of the vacancy cluster decreases. It is noted that no positron lifetime related to carbon vacancies (V_{C}) was observed because almost all V_{C} are reported to disappear upon annealing at about 400 °C.¹⁶ In our case, the implanted wafer was rapid thermal annealed at 850 °C to make V_{C} annealed out.

The variations of magnetization with applied field in the range of $-5 \text{ KOe} < H < 5 \text{ KOe}$ for the implanted sample are displayed in Fig. 2. The magnetization [layer] was related to the mass of a film of 200 nm damaged layer calculated by SRIM program. Diamagnetic (DM) background was carefully calibrated and subtracted. For comparison, M-H curves

TABLE I. The positron lifetimes for the unimplanted and Cu^+ implanted 6H-SiC.

Parameters	Un-implanted	Implanted
τ_1 (ps)	164 ± 3	175 ± 3
I_1 (%)	47.46 ± 0.82	65.80 ± 1
τ_2 (ps)	391 ± 5	406 ± 8
I_2 (%)	46.1 ± 0.82	29.8 ± 1

of un-implanted SiC were also measured, as shown in the inset of Fig. 2, in which the magnetization [sample] was associated with the whole mass of the virgin sample. It is worth stressing that only DM feature can be observed in the unimplanted SiC. After implantation, clear ferromagnetic hysteresis loops were observed at 5 and 300 K, demonstrating the sample exhibits ferromagnetic behavior up to room temperature. The saturated magnetization of Cu -implanted 6H-SiC is about 2.7 emu/g at 5 K, which is slightly larger than that obtained in Ne^+ implanted 6H-SiC.¹⁷ Meanwhile, the coercive field was only about 220 Oe. Such small coercivity was also often observed in TM-doped ZnO or SiC-based DMSs.¹⁸

Many possible factors can cause FM. We first exclude the contribution of copper-related secondary phases because no secondary phases were detected. It has been reported that almost all Cu-based compounds are non-magnetic or diamagnetic.⁷ Although CuO has an antiferromagnetism (AFM) order, it has been excluded from the analysis of the high-resolution of XPS. Besides, an implantation technique is well known as a clean process and thus can avoid the impurity contamination.^{7,19} Recently, vacancy type defects were demonstrated to play a significant role in inducing FM.²⁰ It is, therefore, reasonable to infer that the role of V_{Si} in Cu^+

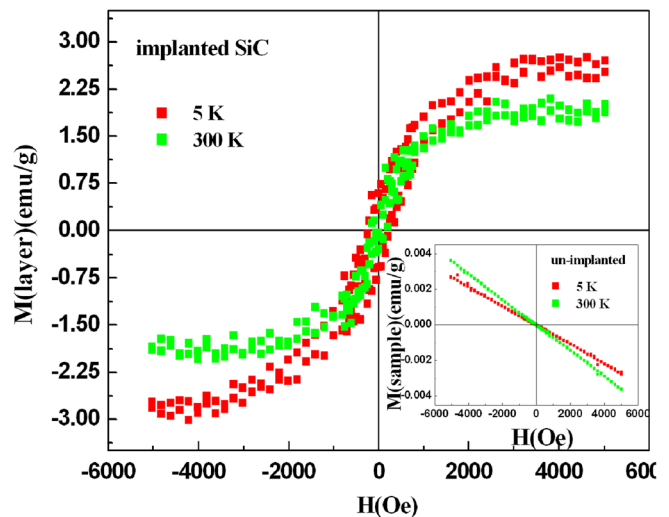


FIG. 2. SQUID hysteresis loops of Cu^+ -implanted 6H-SiC at 5 and 300 K. The magnetization M [layer] was related to a thin layer of 200 nm thickness. Inset is unimplanted 6H-SiC at the same temperatures. The magnetization M [sample] was associated with whole weight of the virgin sample.

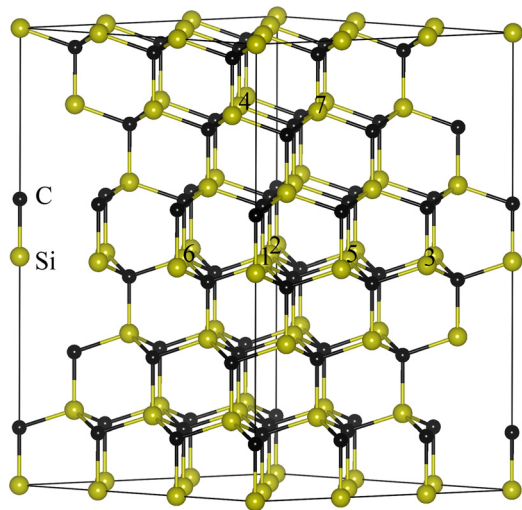


FIG. 3. Side view of $6\text{H-Si}_{52}\text{CuC}_{54}$ and $6\text{H-Si}_{50}\text{Cu}_2\text{C}_{54}$ models.

implanted 6H-SiC is similar to that of nitrogen vacancies in AlN .²¹ In addition, V_{Si} in nitrogen doped SiC can induce FM according to theoretical prediction.²² As mentioned above, the virgin 6H-SiC has only DM feature although V_{Si} measured by the PALS was present, suggesting FM order appears only if the concentration of vacancy exceeds a certain threshold value. Similar defects' threshold effect has also been proposed.^{3,23} Moreover, some Si-C bonds in SiC are changed to Cu-C bonds confirmed by XPS, which will introduce p-d hybridization exchange between Cu and C atoms, resulting in local magnetic moments and exhibit collective magnetization. In short, we propose a possible explanation for the FM origin: the co-effect of substituted Cu along with the implantation induced V_{Si} .

To further explore the origin of FM, we performed the spin-polarized density functional theory (DFT) calculations. The present calculations were implemented using plane-wave pseudopotential method in the Vienna first-principles simulation package (VASP).²⁴ The projector augmented wave (PAW) potentials were adopted, and the general gradient approximation (GGA) PW91 approximation was used to describe the exchange correlation energy.²⁵ A plane wave cutoff of 400 eV was used for the basis set. Following the Monkhorst-Pack scheme, a $3 \times 3 \times 2$ k-point mesh is adopted. The symmetry unrestricted optimizations for geometry are performed using the conjugate gradient scheme until the maximum force allowed on each atom is smaller than 0.02 eV/\AA .

The calculations were carried out by considering two models of $3 \times 3 \times 2$ 6H-SiC supercell, as shown in Fig. 3. The two models of the Cu-doped SiC supercell are based on the experiment: model (1) randomly replacing one Si atom in the supercell by one Cu atom and removing one Si atom ($\text{Cu}_{\text{Si}}\text{-}V_{\text{Si}}$), in which the concentrations of Cu atom and Si vacancy are 1.85 at. \% ; model (2) replacing two Si atoms by two Cu atoms and removing two Si atoms ($2\text{Cu}_{\text{Si}}\text{-}V_{\text{Si}}$), which correspond to a doping concentration of 3.7 at. \% .

First, the magnetism with $\text{Cu}_{\text{Si}}\text{-}V_{\text{Si}}$ is calculated. The calculated total and partial density of states (TDOS and PDOS) for Cu dopant, Si, and C atoms are shown Fig. 4(a). It is observed that the TDOS exhibits a spin-split around the Fermi level, showing the existence of local magnetic moments. It also can be seen from the PDOS of Cu that a marked difference between the spin-majority (occupied) and the spin-minority (unoccupied) states illustrates a notable energy splitting at the Fermi level, giving rise to spin polarization. Both Figs. 4(a) and 4(b) indicate that the magnetic moments mainly come from the $2p$ orbitals of C atoms and $3d$ orbitals of Cu dopant. The calculated result also shows that the total magnetic moment is $2.07\ \mu_{\text{B}}$ per supercell.

Second, the magnetic couplings between $\text{Cu}_{\text{Si}}\text{-}V_{\text{Si}}$ were investigated. In order to find the optimal positions for those two doped Cu atoms and Si vacancies, we studied the following three configurations of the $\text{Cu}_{\text{Si}}\text{-}V_{\text{Si}}$: case 1, substituting Si_1 and Si_2 , removing Si_5 and Si_6 ; case 2, substituting Si_1 and Si_3 , removing Si_5 and Si_6 ; case 3, substituting Si_1 and Si_4 , removing Si_5 and Si_7 (see Fig. 3). The relative energies of the states between FM and AFM ($\Delta E_m = E_{\text{AFM}} - E_{\text{FM}}$) were estimated to be 19 , 65 , and 109 meV for cases 1, 2, and 3, respectively, suggesting the farther the distance between the Cu impurity and Si vacancy, the more stable the ferromagnetic order in $2\text{Cu}_{\text{Si}}\text{-}V_{\text{Si}}$ system. From Table II, we also find that the total magnetic moments for the three cases are 2.25 , 2.49 , and $2.84\ \mu_{\text{B}}$, respectively, implying that the presence of double $\text{Cu}_{\text{Si}}\text{-}V_{\text{Si}}$ can give rise to larger magnetic moment than that of single $\text{Cu}_{\text{Si}}\text{-}V_{\text{Si}}$. Therefore, it is suggested that larger magnetic moment may occur with the increasing of the concentration of Cu dopant and Si vacancy in 6H-SiC . Note that although the DFT/GGA method generally fails to reproduce a realistic distribution of substituted Cu atoms and vacancy-types defects, it does give a reasonable description of the magnetic properties of Cu-implanted 6H-SiC .

In conclusion, Cu-implanted 6H-SiC with room-temperature FM was obtained. The HRXRD analysis and XPS

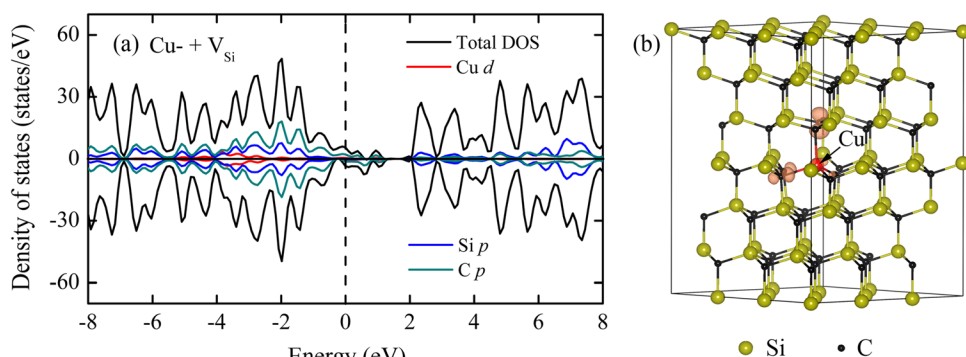


FIG. 4. (a) Total and partial DOSs of $6\text{H-Si}_{52}\text{CuC}_{54}$ with 1.85% Cu substitution and 1.85% Si vacancies. The vertical dotted line indicates Fermi level. (b) Three-dimensional iso-surfaces (the iso-value is 0.02 e/\AA^3) of magnetization density (spin up minus spin down) of $6\text{H-Si}_{50}\text{Cu}_2\text{C}_{54}$ with 3.7% Cu substitution and 3.7% Si vacancies. The yellow balls and black balls represent the Si and C atoms, respectively. The Cu atoms are labeled.

TABLE II. Values of the relative energies of the states between FM and AFM ($\Delta E_m = E_{AFM} - E_{FM}$) and the total net magnetic moments (M_{tot}) calculated for the SiC with 3.7% Cu substitutions and 3.7% Si vacancies.

Complex	Case	ΔE (meV)	M_{tot} (μ_B)
Cu _{Si} + V _{Si}	Case 1	19	2.25
	Case 2	65	2.49
	Case 3	109	2.84

results reveal that no ferromagnetism-related secondary phase appeared. V_{Si} is found to dominate in defects after the implantation. Our complementary experimental and theoretical results suggest that that the substituted Cu along with the irradiation induced vacancies type defects play an important role in FM. This observation could provide a vital clue in understanding the mechanism of ferromagnetism in SiC-based DMSs by implantation.

The authors would like to thank Dr. Renkui Zheng at Shanghai Institute of Ceramics, CAS for his help in HRXRD measurement. This work was supported by the NSFC under Grant Nos. 50802023, 51021091, 11175171, and U1204112, research projects of the scientific and technological department of Henan Province (102102210115), the Scheme of Backbone Youth Teachers in University of Henan Province, Postdoctoral Science Foundation of China, Program for Innovative Research Team in Science and Technology in University of Henan Province (2012IRTSTHN004) and the National Basic Research Program of China (Contracts Nos. 2012CB922003).

¹D. Kitchen, A. Richardella, J. M. Tang, M. E. Flatte, and A. Yazdani, *Nature* **442**, 436 (2006).

²W. B. Mi, E. Y. Jiang, and H. L. Bai, *Acta Mater.* **56**, 3511 (2008).

³Y. Liu, G. Wang, S. C. Wang, J. H. Yang, L. Chen, X. B. Qin, B. Song, B. Y. Wang, and X. L. Chen, *Phys. Rev. Lett.* **106**, 087205 (2011).

⁴K. Bouziane, M. Mamor, M. Elzain, Ph. Djemia, and S. M. Chérif, *Phys. Rev. B* **78**, 195305 (2008).

⁵H. Wang, C. F. Yan, H. K. Kong, J. J. Chen, J. Xin, and E. W. Shi, *Appl. Phys. Lett.* **101**, 142404 (2012).

⁶N. Theodoropoulou, A. F. Hebard, S. N. G. Chu, M. E. Overberg, C. R. Abernathy, S. J. Pearton, R. G. Wilson, J. M. Zavada, and Y. D. Park, *J. Vac. Sci. Technol. A* **20**, 579 (2002).

⁷J.-H. Lee, I.-H. Choi, S. Shin, S. Lee, J. Lee, C. Whang, S.-C. Lee, K.-R. Lee, J.-H. Baek, K. H. Chae, and J. Song, *Appl. Phys. Lett.* **90**, 032504 (2007).

⁸J. Zhou, H. M. Li, L. J. Zhang, J. Cheng, H. F. Zhao, W. S. Chu, J. L. Yang, Y. Luo, and Z. Y. Wu, *J. Phys. Chem. C* **115**, 253 (2011).

⁹C. L. Zhao, C. M. Zhen, Y. Z. Li, L. Ma, C. F. Pan, and D. L. Hou, *Solid State Commun.* **152**, 752 (2012).

¹⁰L. L. Sun, F. W. Yan, H. X. Zhang, J. X. Wang, Y. P. Zeng, G. H. Wang, and J. M. Li, *J. Appl. Phys.* **106**, 113921 (2009).

¹¹A. Koshio, M. Shiraishi, Y. Kobayashi, M. Ishihara, Y. Koga, S. Bandow, S. Iijima, and F. Kokai, *Chem. Phys. Lett.* **396**, 410 (2004).

¹²J. Kansy, *Nucl. Instrum. Methods Phys. Res. A* **374**, 235 (1996).

¹³A. A. Rempel, W. Sprengel, K. Blaurock, K. J. Reichle, J. Major, and H.-E. Schaefer, *Phys. Rev. Lett.* **89**, 185501 (2002).

¹⁴G. Brauer, W. Anwand, P. G. Coleman, J. Störmer, F. Plazaola, J. M. Campillo, Y. Pacaud, and W. Skorupa, *J. Phys. Condens. Matter* **10**, 1147 (1998).

¹⁵G. Brauer, W. Anwand, P. G. Coleman, A. P. Knights, F. Plazaola, Y. Pacaud, W. Skorupa, J. Störmer, and P. Willutzki, *Phys. Rev. B* **54**, 3084 (1996).

¹⁶H. Itoh, A. Kawasuso, T. Ohshima, M. Yoshikawa, I. Nashiyama, S. Tanigawa, S. Misawa, H. Okumura, and S. Yoshida, *Phys. Status Solidi A* **162**, 173 (1997).

¹⁷L. Li, S. Prucnal, S. D. Yao, K. Potzger, W. Anwand, A. Wagner, and S. Q. Zhou, *Appl. Phys. Lett.* **98**, 222508 (2011).

¹⁸B. Song, X. L. Chen, J. C. Han, G. Wang, H. Q. Bao, L. B. Duan, K. X. Zhu, H. Li, Z. H. Zhang, W. Y. Wang, W. J. Wang, X. H. Zhang, and S. H. Meng, *J. Magn. Magn. Mater.* **323**, 2876 (2011).

¹⁹B. Zhang, C. C. Chen, C. Yang, J. Z. Wang, L. Q. Shi, H. S. Cheng, and D. G. Zhao, *Nucl. Instrum. Methods Phys. Res. B* **268**, 123 (2010).

²⁰W. B. Mi, H. L. Bai, H. Liu, and C. Q. Sun, *J. Appl. Phys.* **101**, 023904 (2007).

²¹Y. Liu, L. B. Jiang, G. Wang, S. B. Zuo, W. J. Wang, and X. L. Chen, *Appl. Phys. Lett.* **100**, 122401 (2012).

²²M. W. Zhao, F. C. Pan, and L. M. Mei, *Appl. Phys. Lett.* **96**, 012508 (2010).

²³K. Potzger, J. Osten, A. A. Levin, A. Shalimov, G. Talut, H. Reuther, S. Arpaci, D. Bürger, H. Schmidt, T. Nestler, and D. C. Meyer, *J. Magn. Magn. Mater.* **323**, 1551 (2011).

²⁴G. Kresse and J. Hafner, *Phys. Rev. B* **47**, 558 (1993).

²⁵G. Kresse and D. Joubert, *Phys. Rev. B* **59**, 1758 (1999).